© The American Society of Gene & Cell Therapy

Cis-splicing and Translation of the Pre-*Trans*-splicing Molecule Combine With Efficiency in Spliceosome-mediated RNA *Trans*-splicing

François Monjaret[1], Nathalie Bourg[1], Laurence Suel[1], Carinne Roudaut[1], Florence Le Roy[1], Isabelle Richard[1] and Karine Charton[1]

[1]*Généthon, CNRS UMR8587, 1, rue de l'Internationale, Evry, France*

Muscular dystrophies are a group of genetically distinct diseases for which no treatment exists. While gene transfer approach is being tested for several of these diseases, such strategies can be hampered when the size of the corresponding complementary DNA (cDNA) exceeds the packaging capacity of adeno-associated virus vectors. This issue concerns, in particular, dysferlinopathies and titinopathies that are due to mutations in the dysferlin (*DYSF*) and titin (*TTN*) genes. We investigated the efficacy of RNA *trans*-splicing as a mode of RNA therapy for these two types of diseases. Results obtained with RNA *trans*-splicing molecules designed to target the 3′ end of mouse titin and human dysferlin pre-mRNA transcripts indicated that *trans*-splicing of pre-mRNA generated from minigene constructs or from the endogenous genes was achieved. Collectively, these results provide the first demonstration of DYSF and TTN *trans*-splicing reprogramming *in vitro* and *in vivo*. However, in addition to these positive results, we uncovered a possible issue of the technique in the form of undesirable translation of RNA pre-*trans*-splicing molecules, directly from open reading frames present on the molecule or associated with internal alternative *cis*-splicing. These events may hamper the efficiency of the *trans*-splicing process and/or lead to toxicity.

Received 1 July 2013; accepted 12 February 2014; advance online publication 8 April 2014. doi:10.1038/mt.2014.35

INTRODUCTION

Muscular dystrophies (MD) are a group of genetic diseases affecting the skeletal muscle with no treatment to date. Gene transfer strategies using adeno-associated virus (AAV) vector hold great promise for these diseases, and number of studies have shown impressive results in experimental models, paving the way for the first clinical trials that have been performed in the recent years.[1,2] However, one limitation of using AAV vectors is their encapsidation capacity limited to 4.5 kb, preventing the use of AAV-mediated transfer as therapeutic strategy for large cDNAs such as those for dystrophin, the protein implicated in Duchenne MD (DMD). Besides dystrophin, two other causative genes for MD have a size larger than the AAV encapsidation capacity: titin (*TTN*) and dysferlin (*DYSF*).

The *TTN* coding sequence is 100 kb long and contains 363 exons. It induces two major phenotypes when mutated in its C-terminus: tibial MD (TMD; OMIM600334) and limb-girdle MD type 2J (LGMD2J; OMIM608807).[3,4] The C-terminus of TTN is embedded in the M-line of the sarcomere and is coded by the last six exons (Mex1 to Mex6). LGMD2J and TMD mutations have been found exclusively in the last two *TTN* exons. The most frequent mutation described so far is referred to as FINmaj since it is frequent in the Finnish population.[5] TMD presents as an autosomal dominant late-onset distal myopathy with weakness and atrophy of the anterior compartment muscles of the lower leg and arises when the mutation is present on one allele.[6] LGMD2J, a far more severe phenotype, presents as an autosomal recessive early-onset proximal MD and arises when the mutation is present on both alleles.[4–6]

The *DYSF* coding sequence is 6.2 kb long and comprises 55 exons. It causes, when mutated, two major phenotypes: limb-girdle MD type 2B (LGMD2B; OMIM253601), which presents with muscle weakness predominantly in the proximal pelvic muscles, and Miyoshi myopathy (MM; OMIM254130) that affects mostly the distal muscles of the lower limbs.[7,8] To date, more than 600 causative mutations have been reported along the *DYSF* gene (www.umd.be/DYSF/).

The limitation coming from the AAV encapsidation capacity has fostered the generation of numerous alternative strategies to direct gene transfer, such as splicing-mediated RNA *trans*-splicing.[9,10] Splicing-mediated RNA *trans*-splicing creates a hybrid mRNA from two different molecules through a *trans*-splicing reaction mediated by the spliceosome that makes it possible to exchange mutated sequences for normal ones. Most of the *trans*-splicing strategies applied so far have utilized therapeutic RNAs to replace the 3′ part of the transcript to be repaired. In this case, a *trans*-splicing event occurs between the 5′ splice site of an endogenous targeted pre-messenger RNA (pmRNA) and the 3′ splice site of an exogenously delivered pre-*trans*-splicing molecule (PTM). RNA repair through 3′ *trans*-splicing has been reported in a variety of *in vitro* and *in vivo* experimental studies especially recently in genetic disease contexts at different levels.[11–18]

The last two authors contributed equally to this work.

Correspondence: *Isabelle Richard, Généthon, CNRS UMR8587, 1, rue de l'Internationale, 91002 Evry, France. E-mail: richard@genethon.fr*

© The American Society of Gene & Cell Therapy

We have investigated the efficacy of 3′ *trans*-splicing to replace the last or the last three exons of titin with the aim of targeting all the known TMD/LGMD2J mutations and the six last exons of dysferlin which covers about 20% of the currently identified LGMD2B/MM mutations (111 of 633 mutations; www.umd.be/DYSF/). PTMs have shown their ability to *trans*-splice the transcripts of a titin or a dysferlin minigene *in vitro* as well as the endogenous titin transcript in mouse muscular cells. However, we uncovered autonomous PTM translation occurring both *in vitro* and *in vivo*. Such events may have the possibility to be toxic depending on the generated products but give directions toward improvement of the efficiency of the strategy.

RESULTS

Design of *trans*-splicing molecules

The *trans*-splicing approach for titin and dysferlin pmRNA was tested initially *in vitro* in nonmuscular HER911 cells using minigenes coding part of each protein. For this purpose, a minigene encompassing the genomic sequence for the last 5 exons and 4 introns of the mouse titin gene was amplified from the DNA of a mouse model carrying the FINmaj mutation previously described (KI TTN FINmaj)[19] and cloned in frame with a V5 tag (**Figure 1a**). Similarly, a minigene consisting of the genomic sequence from exon 48 to intron 50 followed by the coding sequence of exon 51 to 55 of the human dysferlin gene was cloned in fusion with a V5 tag (**Figure 1b**).

For targeting dysferlin and titin pmRNA, several PTM molecules were synthesized and cloned in an expression plasmid in fusion with a 3xFlag epitope motif. The PTMs have in common to be composed of a binding domain (BD) except for the negative control of the experiments (delta BD: dBD), a 70-bp artificial intron (aI), the targeted wild-type exonic sequences to be exchanged for titin (human *TTN* Mex6 or the last three exons of human *TTN* Mex4-5–6) or for dysferlin (human exons 49–55), and finally, a SV40 pA signal (**Figure 1**). More specifically, the BD of the RTM Mex6 specific for the titin pmRNA was designed to target the mouse intron Min-5 sequence between Mex5 and Mex6 or the mouse intron Min-3 sequence between Mex3 and Mex4 for the PTM Mex4-6 (**Figure 1a**). For dysferlin, the BD of the PTM Dysf was designed to target the intron 48 of the human dysferlin gene (**Figure 1b**).[20] For each approaches, specific oligonucleotides were chosen to analyze the expression of the

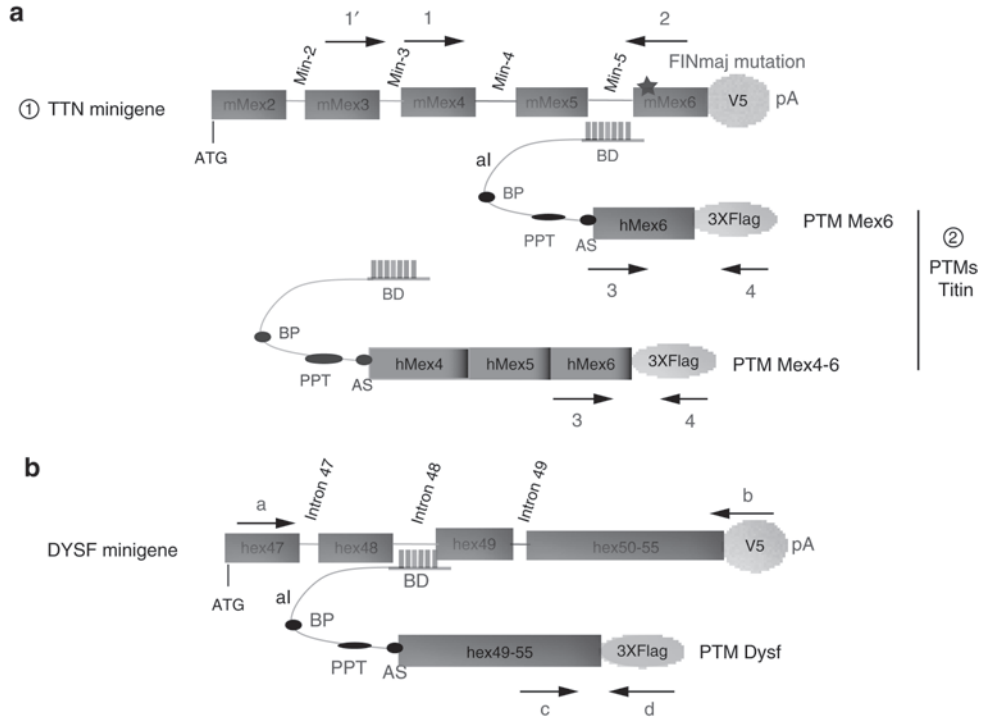

Figure 1 *Trans*-splicing strategy of titin and dysferlin minigenes. (**a**) Diagram of the *trans*-splicing tools used for the 3′ titin exon(s) replacement (please note that the diagram is not drawn to scale). From top to bottom are depicted: : The mouse titin minigene construct used for the experiments in which the last 5 exons and last 4 introns of the mouse TTN gene were fused to a V5 epitope followed by a polyadenylation (pA) signal from SV40. The star symbolizes the presence of the FINmaj mutation. : The titin PTMs Mex6 and Mex4-6 consisting of a binding domain (BD) targeting the titin Min-5 or Min-3 introns, followed by an artificial intron (aI) containing a branching point (BP), a polypyrimidine tract (PPT) and an acceptor site (AS) followed by the WT last or last three exons of human titin fused to a 3xFlag epitope. The location of the oligonucleotides used to discriminate the *trans*-spliced RNA from the minigene and PTM transcripts is indicated by arrows 1-1′-2–3 and 4. Their sequences are given in **Supplementary Table S1**. (**b**) Diagram of the *trans*-splicing tools used for 3′ dysferlin exon replacement. The minigene carries the genomic sequence from exon 47 to intron 49, followed by a merge of the last 6 dysferlin exons fused to a V5 tag followed by a SV40 pA signal. The PTM provides the last 6 exons of dysferlin and carries the same aI as the titin PTM, with a specific BD that targets dysferlin intron 49. The location of the oligonucleotides used to discriminate *trans*-spliced RNA is indicated by arrows **a**, **b**, **c**, and **d**, and their sequences are given in **Supplementary Table S1**.

© The American Society of Gene & Cell Therapy

PTMs, the minigenes and the molecules produced after pmRNA *trans*-splicing (**Figure 1a**,**b** and **Supplementary Table S1**).

The titin and dysferlin minigenes are *trans*-spliced *in vitro*

The minigenes and PTM plasmids were cotransfected in the HER911 cell line using several minigene:PTM ratios (1:3, 1:6, 1:9, and 1:12 for titin PTM Mex6, 1:9 and 1:12 for titin PTM Mex4-6 and 1:5, 1:7 and 1:9 for PTM Dysf). The controls consisted of transfection of the minigene or the PTM alone (with a quantity corresponding to the highest cotransfection ratio), and cotransfection of the minigenes with a PTM where the BD was removed (dBD). Reverse transcription-PCR (RT-PCR) specific for the minigenes, the PTMs, and the expected *trans*-splicing products were performed on RNA extracted 48 hours after transfection.

For the titin and dysferlin experiments, *trans*-spliced RNAs were amplified whatever the ratio of transfected DNAs and the PTMs used, indicating that *trans*-splicing of premessenger titin

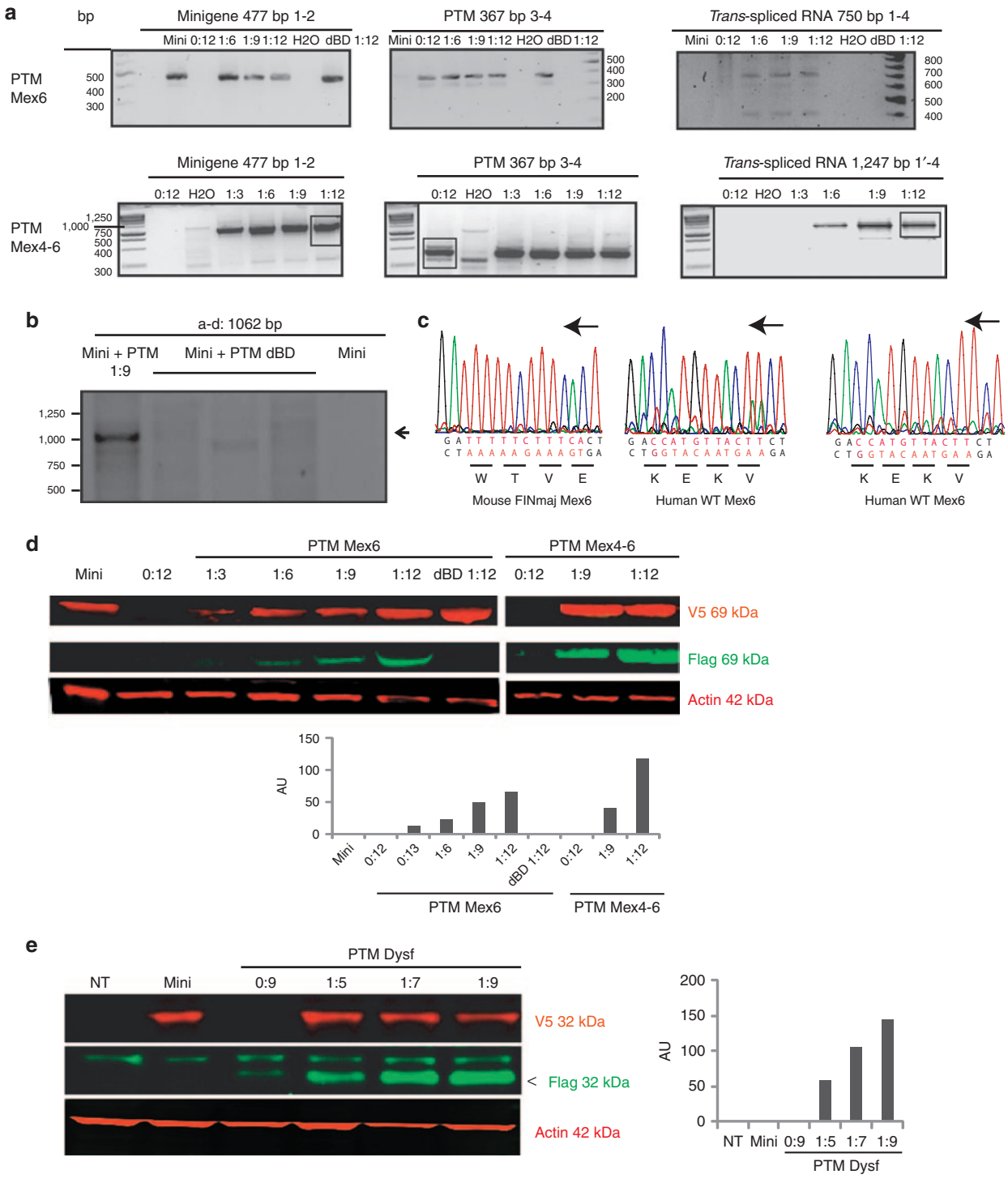

© The American Society of Gene & Cell Therapy

and dysferlin RNA took place. Importantly, *trans*-splicing did not occur when using PTM where the BD was removed (dBD), proving that pairing of the PTM and its target was required for the *trans*-splicing to occur (**Figure 2a,b**). Sequencing of the *trans*-spliced products using the specific Flag oligonucleotide uncovered the expected WT titin sequence, confirming the exchange of the last or the three last exons of titin. As expected, sequencing of the minigene transcript using the V5R oligonucleotide (**Supplementary Table S1**) showed the presence of the FINmaj mutation (**Figure 2c**). Western blots (WB) using a V5 antibody were performed on protein extracts and showed the presence of the miniproteins at the expected size (69 kDa for titin and 32 kDa for dysferlin) in all transfected samples. Labeling with an antibody directed against the Flag epitope (specific for the *trans*-spliced products) revealed the bands at the expected size for all the transfection ratios for PTMs Mex6, PTM Mex4-6, and PTM Dysf but not for the PTM Mex6 and PTM Dysf dBD as expected (**Figure 2d,e**). A relationship between the level of protein translated from the *trans*-spliced RNA and the quantity of transfected PTM expressing plasmids was observed in both cases (**Figure 2d,e**). Interestingly, it seems that increasing the PTM Mex6 quantity played a positive role on the minigene expression, suggesting that the PTM binding can affect the stability of the targeted gene. Taken together, these data indicated that the minititin and minidysferlin *trans*-spliced RNA were correctly translated.

Trans-splicing is efficient on endogenous mRNA *in vitro* and *in vivo*

We next wanted to address the possibility of obtaining *trans*-splicing on endogenous RNA. As a first step, we analyzed the expression of titin and dysferlin mRNA in a number of cell lines including the myogenic C2 cells at the myoblast stage (D0) and after 1 (D1), 2 (D2), and 7 days (D7) of differentiation (data not shown). Detection of titin and dysferlin RNA was obtained only from C2 at all stages. RT-PCR was performed with a set of oligonucleotides (Mex2F and Mex6R for titin and a and 51R for dysferlin, **Supplementary Table S1**). The titin set encompasses the alternatively spliced Mex5 exon. As a control for this RT-PCR, *TA* of WT mouse were amplified and showed the two known alternative spliced isoforms (Mex5+ and Mex5−). The C2 cells at each stage were shown to express dysferlin RNA (**Figure 3a**, left) and almost exclusively the Mex5+ variant (**Figure 3a**, right) as previously shown for some mouse, rabbit, and human muscles.[23] Because the *trans*-splicing is targeting a region of alternative splicing, we hypothesized that the location of the BD could have an important effect. To locate the best site of interaction on titin Min-5, we designed three additional PTMs (PTM1 to 3) only differing from the original one (PTM Mex6) in their BD for targeting different locations on the Min-5 titin intron (**Figure 3b** and **Supplementary Table S2**).

By cotransfection with the titin minigene in HER911 cells, we then verified and compared their *trans*-splicing efficiency. WB for detection of the Flag and the V5 epitopes was performed, and the presence of the *trans*-spliced miniprotein was observed in all conditions, indicating that all PTMs were efficient (**Figure 3c**). From the level of protein obtained, it seemed that the BD giving the best performance of *trans*-splicing is located in the 5′ part of the targeted intron (*i.e.*, PTM Mex6). This observation is in agreement with previous reports showing that targeting the 5′ end of the intron can improve the *trans*-splicing efficiency.[11] In addition, we modified some splicing elements in the PTM Mex6 in an attempt to improve the TS efficiency. First, we introduced by directed mutagenesis, a strong intron splicing enhancer sequence in the chimeric intron of the PTM Mex6. This exon splicing enhancer was described previously as being active in skeletal muscle.[21] Second, we performed silent directed mutagenesis to transform an exon splicing silencer sequence present in the coding sequence into an exon splicing enhancer sequence that is recognized by three different factors as determined by exon splicing enhancer Finder software (**Supplementary Figure S1a**). We performed an *in vitro* experiment in the same conditions than described above using PTMs carrying a single or both modifications (**Supplementary Figure S1b** and **Supplementary Materials and Methods**). WB was performed and quantified, showing that no significant improvement was achieved with the addition of these modifications (**Supplementary Figure S1c**).

To analyze the efficiency of the PTMs on the endogenous pmRNA, we transfected C2 myoblasts with the corresponding plasmids. After 48 hours, cells were scraped and RT-PCR was performed. Results showed the incorporation of the dysferlin Flag sequence (**Figure 3d**, right), and the titin Mex6-Flag in the endogenous C2 titin mRNA regardless of the PTM used. However, the

Figure 2 The titin and dysferlin minigenes are *trans*-spliced *in vitro*. (**a**) RT-PCR performed 48 hours after transfection on HER911 cells using specific oligonucleotides for titin *trans*-splicing (see Figure 1 and **Supplementary Table S1**). The presence of the minigene and pre-*trans*-splicing molecule (PTM) transcripts were detected in the appropriated samples using the 1–2 and 3–4 polymerase chain reaction (PCR), respectively. The presence of a *trans*-spliced RNA was observed for all the minigene:PTM(s) (Mex6, upper panel or Mex4-6, lower panel) cotransfections using the 1–4 or 1′-4 PCR. A control (0:12) was performed with PTM only at the quantity corresponding to the 1:12 ratio and showed no corresponding *trans*-splicing product as expected. (**b**) RT-PCR performed 48 hours after transfection on HER911 cells using specific oligonucleotides for dysferlin TS (see **Figure 1** and **Supplementary Table S1**). The presence of a *trans*-spliced RNA was observed (arrow) in the case of minigene:PTM dysf cotransfection using the a-d PCR. A control (0:9) was performed with minigene only and PTM without binding domain (BD) showed no corresponding *trans*-splicing product as expected. (**c**) The presence of the FINmaj mutation (in red) on the minigene product (left panel) was verified by direct sequencing using the V5R oligonucleotide (**Supplementary Table S1**). The *trans*-spliced product was verified by direct sequencing using the Flag oligonucleotide. The resulting sequence showed the correct WT hMex6 sequence (in red) both for the PTM Mex6 and the PTM Mex4-6 experiment (middle and right panels). Black arrows indicate the orientation of the coding strand. (**d**) Western blot (WB) performed on the cellular extracts transfected with titin PTM, showed the presence of the titin miniprotein at 69 kDa in red (V5 epitope), and the presence of the *trans*-spliced product in green (Flag epitope) from all ratios of transfection. A-actin was used as control. Quantification of *trans*-spliced protein/miniprotein is represented in arbitrary unit (AU). (**e**) WB was performed on HER911 extracts cotransfected with the dysferlin minigene and the PTM Dysf. Labeling using an anti-V5 antibody showed the translation of the minigene into a 32 kDa protein in the corresponding samples (in red). *Trans*-spliced product was detected using the Flag antibody with all minigene:PTM ratios (in green, arrow). A-actin was used as a loading control. Quantification of *trans*-spliced protein/miniprotein is represented in AU. Images were cropped to focus on the proteins of interest. RT-PCR, reverse transcription-PCR.

© The American Society of Gene & Cell Therapy

titin PTM differing by their BD gave a different profile of alternative exon splicing. Indeed, all PTMs induced the synthesis of both Mex5+ and Mex5– titin isoforms but with different relative ratios, while PTM3 led in addition to the synthesis of a new aberrant TTN isoform (**Figure 3d**, right). These results highlight the importance of the BD selection and demonstrate the possibility of modifying the endogenous titin transcript during the splicing reaction. Interestingly, the BD of the PTM Dysf was first designed to target the intron 48 of the human dysferlin gene. Since the BD sequence presents a homology of 62% of the corresponding mouse intronic sequence (**Supplementary Figure S2**), the results obtained indicate that this level of matching is sufficient to obtain recognition for RNA *trans*-splicing.

Finally, following the demonstration of *trans*-splicing *in vitro* on endogenous titin and dysferlin, we investigated whether *trans*-splicing could also be observed *in vivo*. For this purpose, we generated AAV vectors carrying the PTM Dysf (AAV-PTM-hDysf) and the PTM Mex6 (AAV-PTM-Mex6). Intramuscular injections of the AAV coding for the PTM Dysf at the dose of 3.9×10^{12} viral genome (vg)/kg and PTM Mex6 and at the dose of 2.3×10^{12} vg/kg

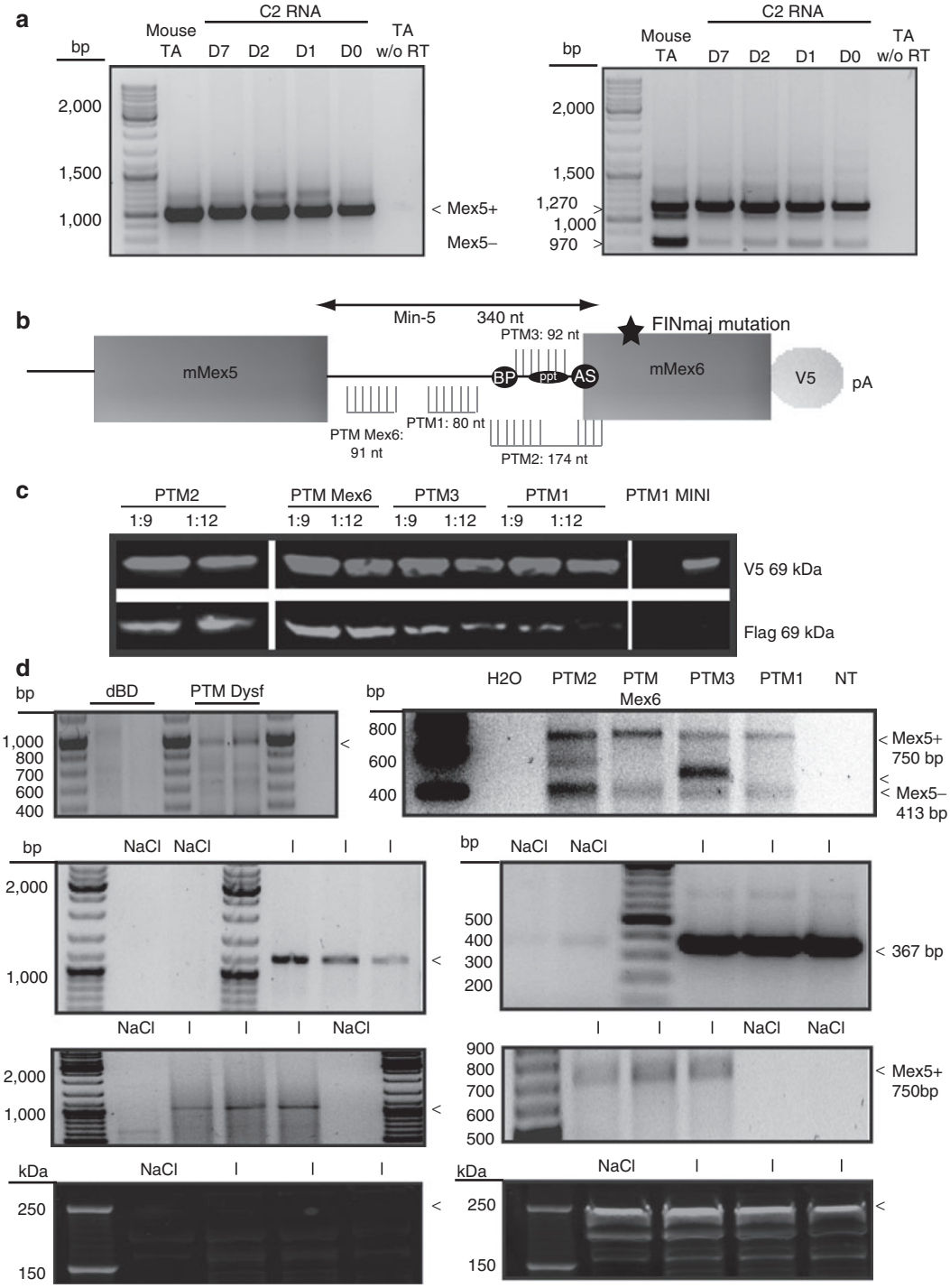

© The American Society of Gene & Cell Therapy

were performed in the tibialis anterior of 1-month-old wild-type male mice. One month after injection, the muscles were sampled and analyzed by RT-PCR, sequencing, and WB. The results showed *trans*-splicing of the endogenous dysferlin and titin pmRNA *in vivo* by RT-PCR (**Figure 3e**). Due to technical difficulty related to the huge size of the titin protein, we investigated the presence of a corresponding protein only for dysferlin. No protein corresponding to the *trans*-spliced RNA was seen at the expected size on WB (**Figure 3f**). These results showed that the *trans*-splicing was successfully obtained *in vivo* at RNA level but suggested that the corresponding protein was not sufficiently expressed from this *trans*-spliced RNA, similarly to what was already reported in other *in vivo trans*-splicing studies.[12,22]

Evidence of an undesired translation of the PTM itself *in vitro* and *in vivo*

Of note, additional bands tagged with the Flag epitope were detected on WB in all the previous experiments, *in vitro* whatever the cell type. The profiles varied between the PTM used but were consistent for each PTM. These bands were detected even under the conditions where PTM or PTM devoid of its BD were transfected alone for the PTM Mex6 and Mex4-6. Indeed, a protein of 16 kDa was visible in all conditions when the titin PTM Mex6 with or without the BD was transfected (**Figure 4a**, left). For the PTM Mex4-6 with or without the BD, protein bands were detected at about 19, 21, and 25 kDa (**Figure 4a**, left). For PTM Dysf, a whole range of specific proteins carrying the Flag tag were seen on WB with the major bands at about 16, 20, 32, 42, 48, and 60 kDa (**Figure 4a**, right).

Similarly, the muscles injected with the AAV carrying the PTM Mex6 and PTM Dysf showed the expression of unexpected proteins (**Figure 4b**). For AAV-PTM Mex6, a protein at 16 kDa similar to the one reported *in vitro* was detected (**Figure 4b**, left). For AAV-PTM-Dysf, WB revealed the presence of proteins at 16, 20, 32, 42, 48, and 60 kDa (**Figure 4b**, right). The six bands correspond to the bands seen *in vitro* after transfection of the PTM Dysf (**Figure 4a**). Therefore, these data confirmed the possibility of PTM to be autonomously translated *in vivo*. Since it was previously reported that AAV-mediated expression of a minidysferlin coding for the first exon and exons 40–55 demonstrated toxicity,[23] we were concerned about the possibility that the expression of PTM-driven proteins may be detrimental. A histomorphological analysis of the injected muscles showed an increase of the fibers presenting centrally located nuclei 1 month after injection in both cases (PTMhDysf and PTM Mex6) (**Figure 4c**).

Confirmation of translation from ORF in the PTM

Since the observed bands were present even when the PTM was transfected alone (with or without the presence of the BD for titin PTM), they seem related to the presence of the PTM but not dependent on *trans* events at the location of binding. A bioinformatics analysis indicated the existence of an open reading frame (ORF) for all PTM sequences in-frame with the Flag epitope and for which the ATG start codon was associated with a predicted Kozak sequence as defined by the ATGPR software (http://atgpr.dbcls.jp/) (**Figure 5a**). In the titin sequence of PTM Mex6, only one such ORF was identified, starting at an ATG embedded in a sequence with a weak predicted Kozak score (ATGPR score 0.10). This ORF would lead to a 6 kDa polypeptide if translated, therefore with a size not consistent with the 16 kDa protein seen on WB. On the PTM Mex4-6, five ORFs were predicted leading putatively to polypeptides of 14, 18, 19, 21, and 25 kDa with respective Kozak scores of 0.19, 0.17, 0.30, 0.23, and 0.31. Three of these putative sequences (18/19, 21, and 25 kDa) may therefore correspond to what was observed on the WB experiment (**Figure 5a**). On the PTM Dysf, six ORFs were predicted that would lead to proteins at 9, 12, 16, 20, 31, and 32 kDa with respective Kozak scores of 0.33, 0.31, 0.13, 0.29, 0.20, and 0.63 (**Figure 5a**). Bands at these sizes, except for the 9 and 12 kDa proteins, were seen on WB, but the predicted ORFs could not account for all observed bands (*i.e.*, 42, 48, and 60 kDa bands; **Figure 5a**).

To verify whether the predicted ORFs could effectively lead to translated products, we performed site-directed mutagenesis transforming ATG into ACG codons. Consistent with the difference between the predicted size and the actual size seen on WB, the mutation of the only ATG of titin PTM Mex6 did not abolish the

Figure 3 Efficiency of *trans*-splicing on endogenous targets. (**a**) dysferlin exons 47–51 RT-PCR with oligonucleotides a to 51R (left) and titin Mex4-6 RT-PCR with oligonucleotides Mex4F to Mex6R (right) (**Supplementary Table S1**) on RNA extracted from WT tibialis anterior (TA) mouse muscle and C2 cells at different days of differentiation D0, D1, D2, and D7. Titin and dysferlin RNA are expressed from the myoblast stage (D0) of C2. Mex5+ and Mex5– were detected in the mouse TA muscle, while the Mex5+ isoform was detected as the major transcript expressed in C2 cells regardless of the differentiation stage. Polymerase chain reaction (PCR) on RNA without reverse transcription was the experimental control. (**b**) Localization and size (nt) of the 4 binding domain (BD) targeting the TTN Min-5 intron used for *trans*-spliced the titin pmRNA. PTM Mex6 contains BDs targeting the 5′ end of the intron Min-5. The BD of the PTM1 targets the middle of the Min-5 intron sequence before the start of the BP. The BD of PTM2 targets the BP and the PPT sequences in the Min-5 intron plus the AS sequence and the first 10 bases of the Mex6 exon. The BD of PTM3 targets the PPT of Min-5. (**c**) Western blot on cell extracts obtained 48 hours after cotransfection of the titin minigene and PTM Mex6, PTM1, PTM2 and PTM3 and PTM1 alone, or minigene alone. Upper: the presence of the mutated V5 tagged miniprotein titin. Lower: the presence of the *trans*-spliced Flag product. The intensity of the green staining depends on the BD used in the PTM to perform *trans*-splicing. Images were cropped to focus on the proteins of interest. Irrelevant lanes were removed. The lanes in each subpanel originate from the same gel. (**d**) RT-PCR using specific oligonucleotides (see **Figure 1** and **Supplementary Table S1**) performed 48 hours after transfection of PTM hDysf or PTM without the BD (left) or titin PTMs (right) on C2 cells at the myoblast stage showed the presence of the dysferlin and titin *trans*-splicing products at the expected sizes. For titin experiment, depending on the localization of the BD, the splicing events in the region are modified. Note the appearance of a band that does not correspond to the Mex5+ or Mex5– isoform when using PTM3. (**e**) RT-PCR performed on RNA extracts from WT TA muscle sections 1 month after injection of AAV-PTM Dysf (right) or AAV PTM Mex6 (left) showed the presence of the PTM Dysf using oligonucleotides BDhdysf4 and d at 1,100 bp and the presence of the PTM Mex6 RNA at 387 bp when injected (upper panel) using oligonucleotides 3 and 4 (**Supplementary Table S1**). The *trans*-spliced dysferlin RNA at 1,000 bp (right) and the *trans*-spliced RNA Mex5+ titin at 750 bp (left) products are shown using oligonucleotides a and d or 1 and 4, respectively (lower panel and **Supplementary Table S1**). (**f**) WB performed on muscles injected with PTM Dysf or injected with physiological saline as control. No Flag-tagged protein corresponding to the endogenous *trans*-spliced dysferlin is seen at the expected size (arrow at 250 kDa, left). Endogenous dysferlin protein is detected at 250 kDa in green, (arrow, right). dBD, delta binding domain; I, injected with PTM; NaCl, injected with physiological saline 0.9% as control. RT-PCR, reverse transcription-PCR.

© The American Society of Gene & Cell Therapy

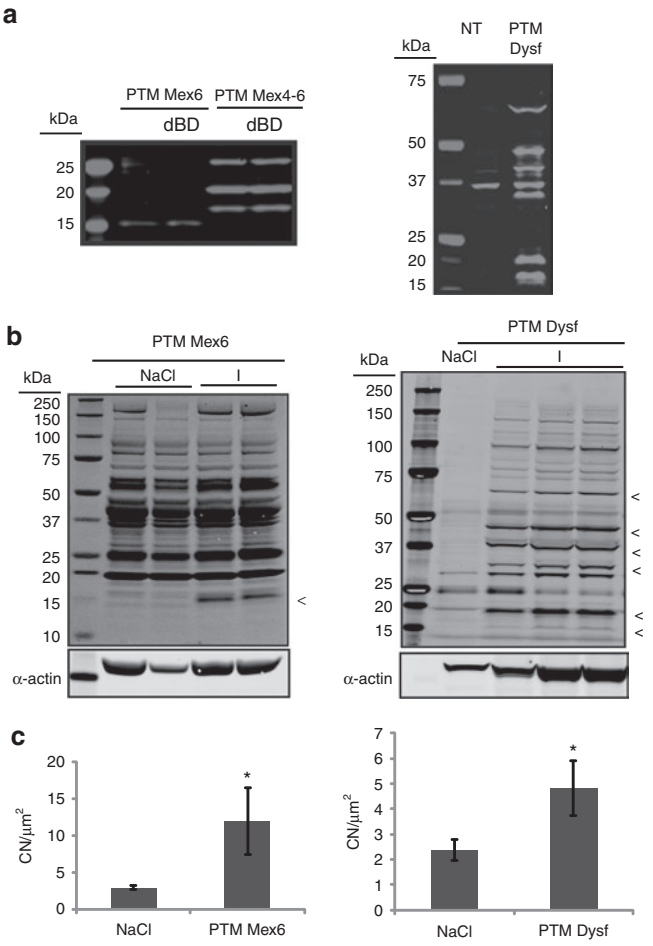

Figure 4 Self-expression of the dysferlin and titin pre-*trans*-splicing molecule (PTMs) *in vitro* and *in vivo*. (**a**) Western blot (WB) performed on HER911 cells transfected by titin PTM Mex6 (left panel), titin PTM Mex4-6 (left panel) and PTM Dysf (right panel). The band at 37 kDa observed both in NT and PTM Dysf conditions is a nonspecific band. Each experiment shows the presence of additional unspecific proteins 48 hours after transfection. dBD, delta binding domain; NT, nontransfected cells. (**b**) Left: WB performed on the protein extracts shows the 16 kDa protein expression with Flag antibody after the PTM Mex6 injection similarly to what was seen *in vitro*. All the other bands observed both in NT and PTM Mex6 conditions are nonspecific as found both in physiological saline and PTM injected muscles. The lanes in each subpanel originate from the same gel. A-actin was used as control. Right: WB performed on protein extracts shows the presence of a number of bands using the Flag antibody which correspond to bands described *in vitro*. The lanes in each subpanel originate from the same gel. A-actin was used as control. (**c**) Centronucleation index was measured (CN/μm²) after histological analysis of the muscle injected with the PTM Mex6 (left) or the PTM Dysf (right) versus physiological saline (NaCl) injection in the contralateral muscle. PTM Mex6 injection induced a process of degeneration/regeneration in the muscle after 1 month of injection. $*P < 0.5$.

expression of the 16 kDa protein, whose origin remained therefore to be determined (**Figure 5b**, top left). In contrast, for the PTM Mex4-6, mutations of ATG start codon of the 21 and 25 kDa ORF (ΔATG25 and ΔATG21) alone or together abrogated the expression of the extra proteins at the corresponding sizes (**Figure 5b**, bottom left). It should be noted that the alteration of the ATG21 induced a large reduction in the 25 kDa protein. For dysferlin, we generated three mutated PTMs: (i) ΔATG20 where the ATG corresponding to the 20 kDa ORF was mutated, (ii) ΔATG32+31 where the first two ATGs corresponding to the ORF predicted to lead to 32 and 31 kDa proteins were mutated together, and finally (iii) Δ4ATG with mutation of all the 4 ATG (*i.e.*, 16, 20, 31, and 32 kDa predicted proteins). The PTM coding proteins seen on WB with the PTM Dysf were partly eliminated by the ATG mutations (**Figure 5b**, right). Indeed, whereas ΔATG20 did not remove any protein expression, ΔATG32+31 removed the protein at 32 kDa and Δ4ATG removed the 16 and 32 kDa proteins. Taken together, these results indicate that some of the proteins generated by the presence of the PTMs in cell were the result of translation of ORFs present in the PTM sequences. Nevertheless, not all the bands were removed, indicating the existence of other(s) mechanism(s) for their generation.

Evidence of *cis*-splicing within the PTM molecules

Since some proteins could not be explained by ORF presence, we investigated the possibility of *cis*-splicing occurrence within the PTM sequence as an underlying mechanism. RT-PCR was performed with oligonucleotides located in the BD (BD1 for titin and BDhdysf1 and 4 for dysferlin) and Flag (**Supplementary Table S1**) after RNA extraction of cells transfected by the corresponding PTMs. The RT-PCR performed after transfection uncovered a major additional band with a size ~850 bp shorter than the full-length amplification for PTM Dysf (**Figure 6a**, top left), and a 150 bp shorter amplification band was observed on agarose gel for PTM Mex6 (**Figure 6a**, bottom left). Sequencing of these bands revealed a 852 bp deletion spanning from the BD to the end of the Dysf sequence and a 141 bp deletion spanning from the BD to the beginning of the hMex6 sequence (**Figure 6a**, right). Examination of the sequences at the site of the junction uncovered, a very weak donor splicing site (DS) with a score of 45.01 for PTM Dysf and a strong cryptic DS with a score of 73.39 for PTM Mex6 (http://ibis.tau.ac.il/ssat/SpliceSiteFrame.htm). The deletion created by the splicing lead to the generation of a new ORF of 405 nt for PTM Mex6, whereas no new ORF appears in the PTM Dysf. Translation of the corresponding product would result in a 15 kDa protein in-frame with the Flag tag, therefore accounting for the band observed on WB after PTM Mex6 transfection. To verify that this sequence was indeed used as a DS, we modified it by directed mutagenesis (GT -> GA) and analyzed the consequence on splicing after the transfection experiment using the modified PTM (PTM Mex6—DS1). RT-PCR showed the removal of the additional splice event, confirming that the sequence was indeed a cryptic DS and demonstrating that splicing could occur within the PTM sequence (**Figure 6b**).

We complemented this analysis by a RNA-seq experiment using RNA extracted from cells transfected by the PTM Mex6. The total number of reads mapped to the PTM genome was 71,680. Junction analysis identified a total of 33 potential splicing junctions within the molecule with 29 of them supported by a minimum of 3 junction reads (**Figure 6c**). Seven of the splice junction sites were present in more than 150 reads, including the event identified by RT-PCR which corresponded to the main form by far (16,881 reads versus 1,388 for the second major event). Approximately 36% of all splicing sites conformed to the consensus sequence GT/AG. However, more than 39% of

© The American Society of Gene & Cell Therapy

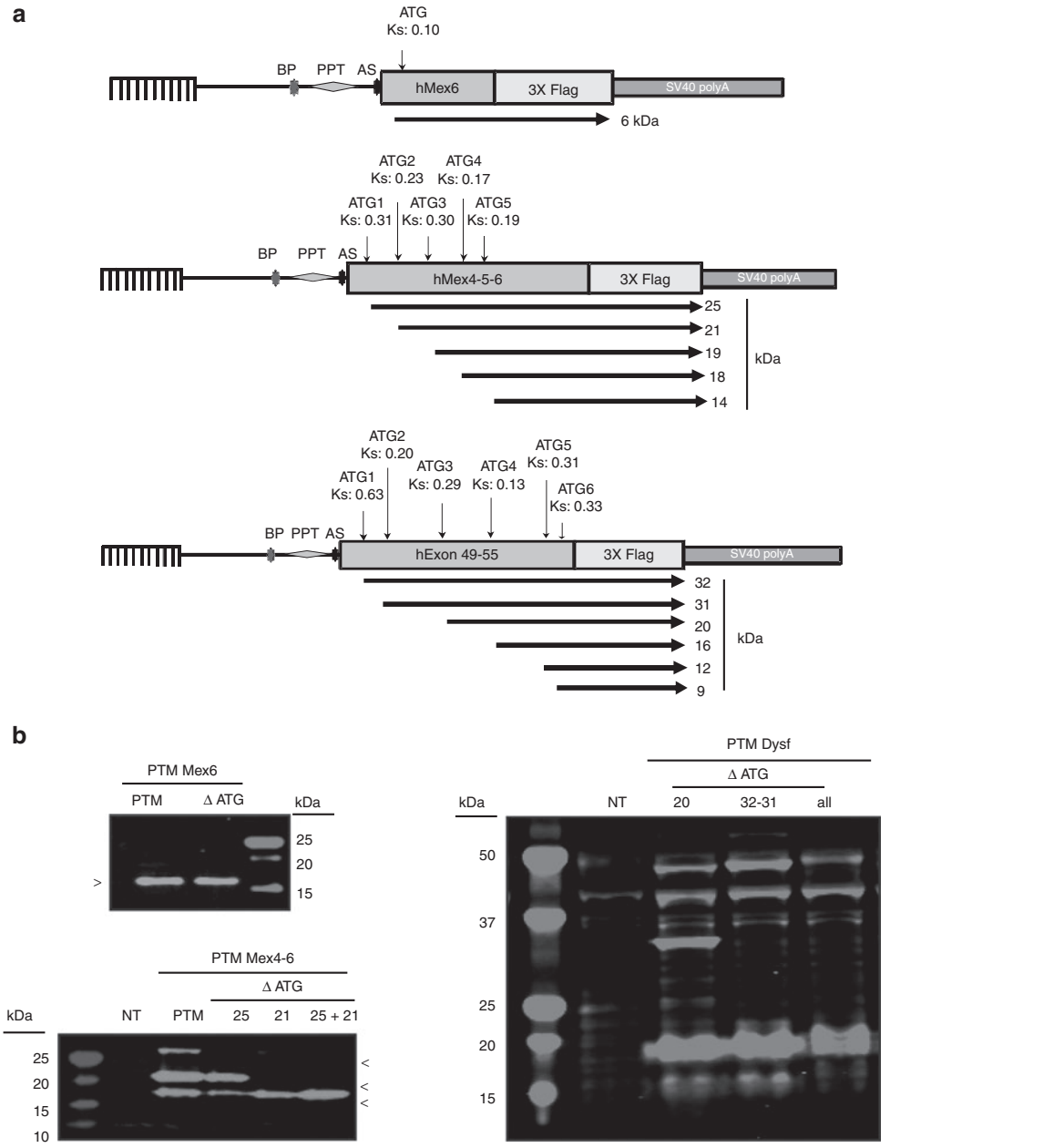

Figure 5 Confirmation of translation from an open reading frame (ORF) present on the pre-*trans*-splicing molecule (PTM). (**a**) Location of the ORF relative to the PTM sequences. Each ORF with a significant Kozak score as defined by ATGPR software is indicated by an arrow below the diagram of each PTM. The position of the ATG, the Kozak score (Ks), and the corresponding predicted polypeptide weight is also indicated. AS, acceptor site; BP, branching point; PPT, polypyrimidine tract. (**b**) Analysis of the consequences of mutation of the ATG in the PTM. Left panel (top): western blot (WB) performed on HER911 cells transfected by titin PTM Mex6 or PTM Mex6 ΔATG. This experiment demonstrates that the observed 16 kDa protein is not translated from the corresponding ATG. Left panel (bottom): WB performed on HER911 cells transfected by titin PTM Mex4-6 or the PTM depleted of a different ORF initiating ATG (ΔATG25 or 21, or both 25+21). These ATG mutations abolished the proteins at 25 or 21 kDa or both, respectively. Right panel: WB performed on HER911 cells transfected by PTM Dysf or PTM Dysf depleted of the first two ATG (ΔATG32+31), the third ATG (ΔATG20), and finally, the ATG32, 31, 20, and the fourth ATG (ΔATGall). Disruption of ATG32 and 31 led to the disappearance of the 32 and 31 kDa proteins, respectively. ATG20 disruption does not show any protein disappearance on WB. The ATG16 disruption leads to the disappearance of the 16 kDa protein.

the junction sites belonged to the most common nonconsensus splice junction GC/AG, while 12% corresponded to GT/AG, and the rest of the splice junction sites represented GA/AA, GC/GT, AT/AA, or AT/CA splice junction (~3% each). The sequence of the exon–intron (donor) and intron–exon (acceptor) splice sites were extracted and used to compute the nucleotide frequency at each position. Overall, this analysis uncovered no real consensus splice site but only conservation at the +1+2 or −2/−1 consensus dinucleotide. The preeminent signature consisted of a T at +2 for DS and a A at −2 for AS, indicating that these bases are the main determinant of splicing (**Figure 6d**).

© The American Society of Gene & Cell Therapy

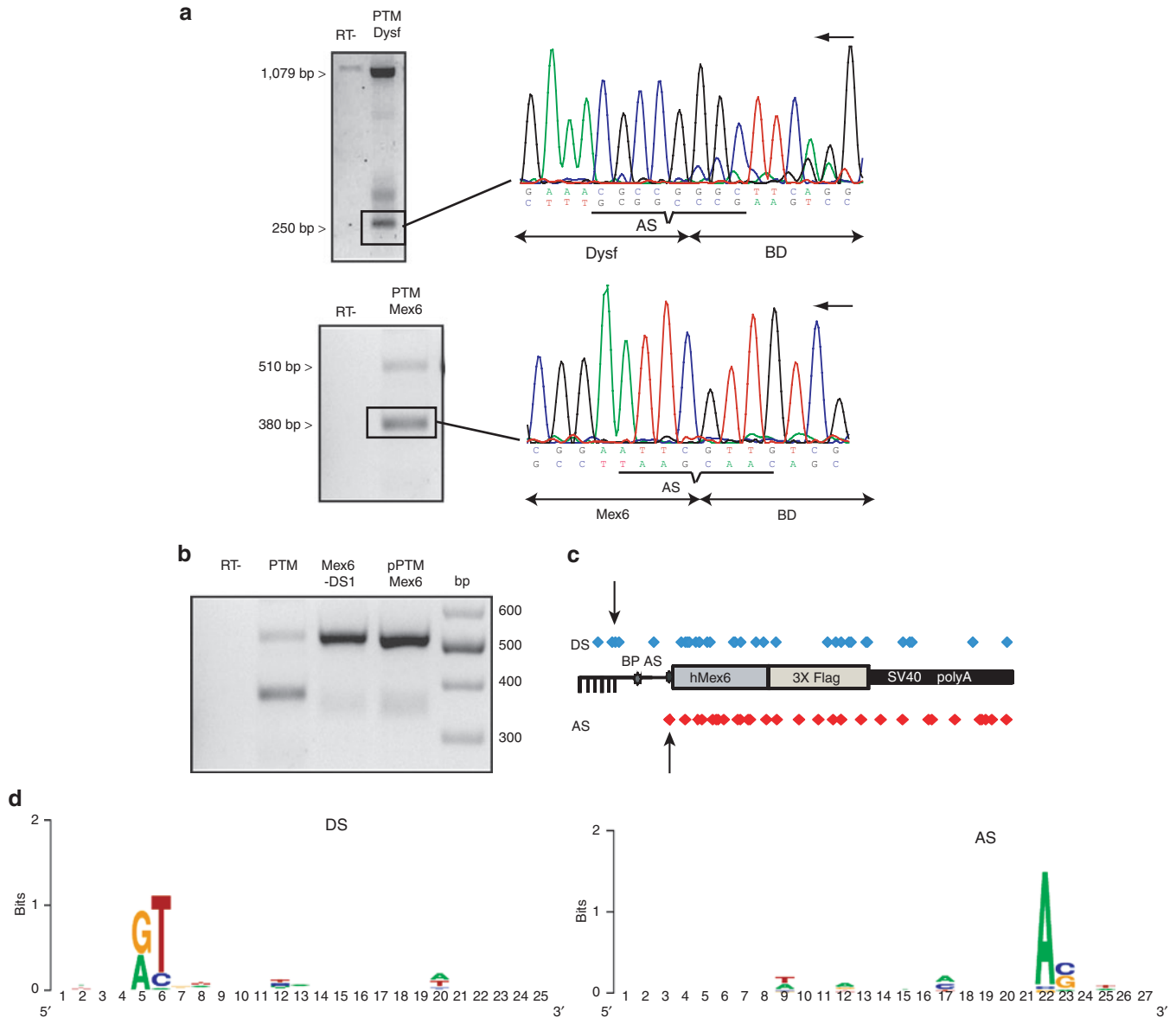

Figure 6 ***Cis*-splicing occurred within the pre-*trans*-splicing molecule (PTM) RNA sequence.** (**a**) RT-PCR was performed between the beginning of the BD sequences using oligonucleotides BD1 on the PTM Mex6, the oligonucleotides BDhdysf4 on the PTM Dysf and oligonucleotide 4 located in the Flag tag sequence (**Table S1**). **(a)** Top: RT-PCR performed on RNA extracted from cells transfected by PTM Dysf. The negative control consisted of the experiment performed without the RT. Amplification of a full-length RNA (1127 bp) and a smaller RNA at 268 bp (box) was observed. Bottom: RT-PCR performed on RNA extracted from cells transfected by PTM Mex6. Amplification of the full-length RNA (550 bp) and a smaller RNA at 400 bp (box) was observed. The negative control consisted of the experiment performed without the RT. Sequencing of the small transcripts (the black arrow indicates the orientation of the coding strand) (**Supplementary Table S1**) shows *cis*-splicing between the predicted DS and the AS present in PTM Dysf (top) and in PTM Mex6 (bottom). (**b**) RT-PCR performed on RNA extracted from cells transfected by PTM Mex6 with or without the predicted DS. PTM Mex6 induces the production of a full-length RNA (550 bp) and a smaller RNA missing about 150 bp (box). Modification of the DS (PTM Mex6-DS1) prevented the production of this form. The plasmid PTM-Mex6 is used as the positive control. (**c**) A RNA-seq experiment identified a large number of alternative splicing events. Each dot in blue represents a donor splice site identified by RNA-seq and each dot in red represents an acceptor splice site. The two series of dots are aligned along the representation of the PTM Mex6. The two arrows indicate the splicing sites corresponding to the most frequent event. (**d**) Logos plots of the consensus sequences encompassing the DS and AS identified in the analysis generated using http://weblogo.berkeley.edu/logo.cgi. RT-PCR, reverse transcription-PCR.

DISCUSSION

In this study, we tested the *trans*-splicing strategy for two large MD-related genes (*TTN* and *DYSF*). We demonstrated the possibility of specifically exchanging exon(s) during the splicing reaction in titin and dysferlin minigenes and endogenous transcript *in vitro* and *in vivo*. In the process of obtaining these positive results, we uncovered issues related to the *trans*-splicing strategy: (i) modification of alternative splicing following binding of the PTM on its target and (ii) generation of polypeptides from direct translation of ORFs in the PTM sequence or following *cis*-splicing of the PTM.

Although it has never been reported to occur in a *trans*-splicing strategy, it is not surprising that binding of the PTM to

© The American Society of Gene & Cell Therapy

its intronic target can induce alteration in the splicing equilibrium since it may mask regulatory splicing sequences such as the PPT or the BP. This is in fact the principle on which the exon-skipping method is based. This possibility calls for a careful evaluation of the binding region when designing a PTM. This is further strengthened by the fact that we were able to show that a BD with 62% of homology to its target could induce efficient *trans*-splicing *in vivo*, leading to the possibility that increasing the length of the BD induces potential off-targets as previously suggested.[24,25] What was more surprising is the extent of alternative splicing observed within the PTM. Regular RT-PCR analysis uncovered major alternative forms joining cryptic DSs present within the BD to the strong AS introduced in the construct at the beginning of the coding sequence in the PTM. The existence of such event was confirmed by RNA-seq for Mex6. In addition, this analysis showed the potential of the PTM RNA molecule to generate a large range of alternative transcripts. These events are probably rendered possible by the presence of the splicing factors recruited by the strong AS present in the PTM. Interestingly, conservation analysis of the splice junctions revealed that the cryptic sites that were used can deviate largely from the canonical consensus sequences of splice sites. In fact, there is no real homology apart from the dinucleotide classically found at the 5′ and 3′ ends of introns. It appears from this analysis that a major determinant for splicing is the presence of a T at +2 in the DS and an A at −2 in the AS. As we demonstrated, it is possible to prevent the generation of major aberrant *cis*-spliced products by silent mutagenesis. However, the absence of consensus would preclude the total elimination of this problem although it would be possible to minimize further the formation of abnormal events by eliminating as much as possible A and T.

Besides the *cis*-splicing that would diminish the molecules available for *trans*-splicing, we also showed that the PTM can be translated on its own directly from ORFs present in the PTM or following *cis*-splicing. Furthermore, our observations are probably only the tip of the iceberg. Indeed, only the protein products in frame with the Flag tag are observed on WB, but it is quite possible that other polypeptides can be expressed from the two other phases (with or without internal *cis*-splicing) and remain undetected. Surprisingly, despite the number of publications on 3′ *trans*-splicing strategies, PTM translation is an issue that is rarely highlighted or discussed, probably because this possibility has not always been investigated. Indeed, this would necessitate an *in vitro* condition where the PTM was transfected alone in the absence of the target sequence and an analysis of the protein expression using an antibody directed to the C-term part. In addition to our observation, evidence of PTM translation itself was noticed in only one case in an experiment using a LacZ reporter gene.[24] While the authors indicated that translation of PTMs is a potential problem that should be addressed, they did not investigate the mechanism of the generation of the aberrant products. In our case, we clearly demonstrated that some of the products that were generated came from translation of a direct ORF or ORF generated following *cis*-splicing. Again, it would be possible to use mutagenesis to reduce the presence of ORF but their total elimination would require modifying the amino acid sequence. Therefore, it would be of interest to develop strategies to prevent the possibility of translation such as preventing the export of the RNA to the cytoplasm.

Our observations also raise specific concerns of toxicity since 1 month of injection of the PTM demonstrated increase of the centronucleation index. First, toxicity could be related to deregulation of endogenous alternative splicing such as that observed in the case of titin. *In vivo*, the levels of inclusion of Mex5 vary between different skeletal muscles,[26] and respecting the ratio may be of importance, especially since the is7 domain encoded by Mex5 carries/includes a calpain 3 binding site suggesting that the is7− and + titin isoforms may have different properties. Secondly, the generation of aberrant polypeptide products raises the possibility of toxicity coming either from an immune reaction against non-self-molecules or from the nature of the products themselves. In the case of dysferlin, for example, previous reports indicated that expression of a minidysferlin whose structure was close to our PTM could generate cytotoxicity.[23]

In conclusion, we showed that, in addition to achieve *trans*-splicing, the transfer of a PTM can lead to unwanted events in the form of *cis*-splicing or translation from ORF. Modifying (in as much as possible) the DS and ORF present in the PTM sequence is one mandatory step, but developing means to prevent the transport of the PTM RNA into the cytoplasm would be of utmost interest. We propose also that the understanding of the mechanisms involved could shed some light on the reasons underlying the weak efficiency of protein generation generally observed in *trans*-splicing strategies. This may therefore open the door to improvement in engagement of an increased percentage of the PTM RNA molecules in the *trans*-splicing reaction and may therefore help to put TS closer to the clinic. It appears also essential to carefully evaluate the possibility of toxic products generated from the introduction of the PTM molecule, to create systems preventing the PTM splicing and translation, and consequently, to offset the risk/benefit of this approach before clinical use.

MATERIALS AND METHODS

Cloning

Minigenes. All polymerase chain reaction (PCR) products were generated with either REDTaq (Sigma, St Louis, MO) or Phusion (NewEngland Biolabs, Ipswich, MA) DNA polymerase. Two minigenes coding part of the titin and dysferlin genes were constructed. The titin minigene covers the last five exons (Mex2 to the last amino-acid coding codon in Mex6) of the murine titin gene and carries the FINmaj mutation. It was obtained by specific PCR amplification (oligonucleotides Mex2F/Mex6R, **Supplementary Table S1**) on tail DNA from a knock-in TTN FINmaj mouse[19] and cloned into the pcDNA3.1.TOPO.V5.His plasmid (Life Technologies, St Aubin, France). The resulting plasmid pDNA3.1.TOPO.V5.His Mex2-6 DNA FINmaj expresses a minititin protein fused at its C-terminus with a V5 epitope under the transcriptional control of the cytomegalovirus (CMV) promoter. The dysferlin minigene comprises the human genomic sequence (ENSG00000135636) from exon 47 to intron 50 followed by the Human cDNA from the beginning of exon 51 to the last amino-acid coding codon in exon 55 (hDysferlin cDNA var8, NM 003494.3). It was obtained by DNA synthesis (Genecust, Luxembourg) and cloned in a SPc5-12 promoter-driven plasmid[27] in fusion with a V5 epitope at its C-terminus.

PTM plasmids. A first titin PTM sequence (PTM Mex6) that includes a BD, an artificial intron (aI) containing a spacer sequence,[28] the human titin Mex6 exon (hMex6), three copies of a Flag epitope (3xFlag; Sigma), and a SV40 polyadenylation signal was synthesized by Genescript (Piscataway, NJ), and the sequence was cloned in a CMV promoter-driven plasmid. The BD was framed between two restriction sites

© The American Society of Gene & Cell Therapy

(BamH1 and SacII) for complete deletion or an easy exchange with other BDs (**Supplementary Table S2**) designed to be specific for a different part of the targeted intron and obtained by synthesis (Genecust). The second PTM contains the same elements but carries the titin human exons hMex4-5 and 6 and was cloned in a SPc5-12 promoter-driven plasmid.

The dysferlin PTM (PTM Dysf) sequence is composed of a BD complementary to 249 bp of intron 48 of the human DYSF gene, the aI and the last seven exons (49–55) of the human dysferlin, cloned in-frame with a 3xFlag motif. The PTM Dysf sequence was obtained by DNA synthesis (Genecust) and cloned in a SPc5-12 promoter-driven plasmid (pSPc5-12PTMhDysf). All plasmids were prepared using the EndoFree plasmid kit (Qiagen, Hilden, Germany) and sequenced.

Directed mutagenesis. Site-directed mutagenesis was performed to mutate ATG into an ACG codon or the donor site (GT -> GA) in the PTM Mex6. Mutagenesis was achieved using the Quikchange site-directed mutagenesis kit (Agilent Technologies, Santa Clara, CA) following manufacturer instructions and using home-designed oligonucleotides (**Supplementary Table S3**). All mutated plasmids were prepared using the EndoFree plasmid kit (Qiagen) and sequenced.

AAV vector production. Adenovirus-free rAAV2/8-pSPc5-12PTMhDysf and rAAV2/9-pCMVPTMMex6 viral preparations were generated by packaging AAV2-inverted terminal repeat region recombinant genomes in AAV8 or 9 capsids using a three plasmid transfection protocol. Viral genomes were quantified by a TaqMan real-time PCR assay using primers and probes corresponding to the inverted terminal repeat region of the AAV vector genome. The primer set and TaqMan probe used for inverted terminal repeat region amplification were: 1AAV65/Fwd: 5′-CTCCATCACTAGGGGTTCCTTGTA-3′; 64AAV65/rev: 5′-TGGCTACGTAGATAAGTAGCATGGC-3′; and the probe AAV65MGB/taq: 5′-GTTAATGATTAACCC-3′.

Cell culture and transfection. The human embryonic retinoblast HER911 and mouse myogenic C2 cell lines obtained from the American Type Culture Collection (Molsheim, France), were cultured in Dulbecco's modified Eagle's medium (Life Technologies) supplemented with 10% fetal bovine serum (Sigma), 10 µg/ml of gentamicin (50 mg/ml, Life Technologies), plus 0.1% NEAA MEM for HER911 cells (Sigma).

HER911 and C2 cells were transfected using FuGENE HD (Promega, Madison, WI). A day before transfection, cells were plated in six-well plates or 10-cm dishes. Cells at 80–90% of confluence (HER911) and 60% confluence (C2) were transfected either the minigene plasmid alone or the minigene plus different concentrations of the PTM plasmid of interest, or PTM alone, using 4 µl of of FuGENE HD transfection reagent per microgram of DNA as indicated by the manufacturer's protocol. The amount of transfected DNA was standardized between the different conditions of the same experiment using DNA from a noncoding plasmid. Cells were scraped 48 hours after transfection in the culture medium and centrifuged at 500*g*, at 4 °C for 5 minutes. The cell pellet was stored at −80 °C until use.

In vivo *experiments.* All procedures on animals were performed in accordance with the directive of 24 November 1986 (86/609/EEC) of the Council of the European Communities and were approved by Genethon's ethics committee under the number CE-11–013. Animals were housed in a barrier facility with 14-hour light, 10-hour dark cycles, and provided food and water *ad libitum*. C57BL/6 mice were purchased from Charles River Laboratories (L'Arbresle, France).

For *in vivo* experiments assessing AAV-mediated PTM Dysf or PTM Mex6 expression in 1-month-old C57BL/6 mice, rAAV2/8-pSPc5-12PTMhDysf or rAAV2/9-pCMVPTM Mex6 viral preparations were injected into the left *TA* (3.9×10^{12} and 2.3×10^{12} viral genome (vg)/kg, respectively), the collateral muscle was injected with physiological saline (NaCl, 0.9%). One month later, mice were sacrificed and tissue specimens immediately collected, snap frozen in liquid nitrogen–cooled isopentane and stored at −80 °C.

RNA analysis. Total RNA was extracted from cell pellet or muscle sections using Trizol reagent (Life Technologies) after homogenization and treatment by DNase (Life Technologies) for 2 hours at 37 °C. RNA was quantified using a Nanodrop spectrophotometer (Thermo Scientific, Illkirch, France) and diluted with UltraPure DNase/RNase-free distilled water (Life Technologies) to 0.125 µg/µl. Synthesis of cDNA was performed from 1 µg of total RNA using the Verso cDNA kit (Thermo Scientific) with a mix of oligo-dT and random primers for 1 hour at 42 °C. Regular nonquantitative PCR was performed on 10 µl of cDNA with oligonucleotides specific for the corresponding PTM, minigene, endogenous transcript, or *trans*-splicing products (**Supplementary Table S1**) using RedExtract N-AmpTM PCR Ready MixTM (Sigma). PCR to determine *cis*-splicing was performed with oligonucleotides presented in **Supplementary Table S1** called BD1 for PTM Mex6 and BDhDysf1—BdhDysf4 for PTM Dysf and oligonucleotide 4. For all PCR, samples were amplified for 34 cycles, each consisting of denaturation at 98 °C for 10 seconds, annealing at 54 °C for 30 seconds, and elongation at 72 °C for 45 seconds followed by final amplification at 72 °C for 10 minutes. The resulting amplicons were analyzed by gel electrophoresis and/or direct DNA sequencing using the oligonucleotides located in the Flag sequence (oligonucleotide 4) or V5R oligonucleotide (**Supplementary Table S1**).

RNA-seq analysis. Libraries were prepared using the TruSeq RNA Sample kit according to the recommendations of the supplier (Illumina, San Diego, CA). Briefly, the steps of this protocol are: capture of polyA+ mRNA using oligo dT beads from 5 µg of total RNA, fragmentation at a size of 400 nt by sonication synthesis of the double-stranded DNA, ligation of Illumina adapters, and PCR amplification of the library. Paired-end sequencing on 100 bp was then run on Illumina HiSEQ 2000. Bioinformatical analysis of the sequencing data was performed as described in ref. 29 in four steps: (i) alignment of the reads on the reference genome (mm^9) supplemented by the exogenous sequence of the PTM using the TopHat2 software,[30] (ii) detection, assembling, and quantification of the sequenced transcripts using the Cufflinks software,[31] and (iii) detection of fused transcripts using the TopHat-Fusion software.[32] Examination of the data was performed through the web interface Integrated Genome Viewer (http://www.broadinstitute.org/igv/), and graphic representation of the consensus sequence around junctional sites were obtained using the web-based tool WEBLOGO (http://weblogo.berkeley.edu/logo.cgi).

WB analysis. For *in vitro* and *in vivo* experiments, cell pellet and muscle tissue sections were mechanically homogenized in a lysis buffer containing 20 mmol/l of Tris HCl pH 7.5, 150 mmol/l NaCl, 2 mmol/l EGTA, and 0.1% TritonX-100 supplemented with complete mini protease inhibitor cocktail (Roche, Basel, Switzerland).

After centrifugation (14,000*g*, 4 °C, 10 minutes), samples were mixed with DTT (1 mmol/l final, Sigma) and NuPAGE (1X final) loading buffer (Life Technologies). Protein samples were denaturated at 70 °C for 10 minutes and loaded on precast 4–12% Bis–Tris polyacrylamide or 3–8% Tris–acetate NuPAGE gradient gels (Life Technologies). Electrophoresis was performed for 1 hour at 180 V. Transfer was performed onto PVDF membranes (Millipore, Billerica, MA) 1 hour at 100 V or 8.5 minutes using i-Blot system (Life Technologies). The membrane was blocked for 45 minutes with blocking buffer (Li-cor, Lincoln, NE) and incubated for 1 h at room temperature with the indicated dilution of primary antibody: Rabbit monoclonal anti-V5 (1:1,000) (Life Technologies), mouse monoclonal anti-Flag (1:1,000) (Genetex, Hsinchu City, Taiwan), rabbit anti-Flag (1:200) (Sigma), anti-Dysferlin NCL-Hamlet antibody (1:500) (Leica Biosystems, Nanterre, France), and Rabbit α-actin 1 (1:1,000) (Sigma, A2066) diluted in blocking buffer. After washing three times with TTBS (50 mmol/l Tris, 138 mmol/l NaCl, 2.7 mmol/l KCl pH 8.0, 0.01 % Tween

© The American Society of Gene & Cell Therapy

20), the membrane was incubated at room temperature for 1 hour with either goat anti-rabbit or goat anti-mouse Odyssey secondary antibodies (1:10,000) (Li-cor) coupled to a 700 or 800 nm. Immunolabeled proteins were detected using the Odyssey Infrared Imaging System (Li-cor). Quantifications were performed using the Odyssey Application Software.

Histological analysis. Cryosections (8 µm thickness) were prepared from frozen muscles injected or noninjected by the AAV-PTM Mex6 or AAV-PTM Dysf. Transverse sections were processed for Hematoxylin-Phloxin-Saffron and imaged using a Nikon Eclipse E600 microscope with a charge-coupled devices camera (Sony, Tokyo, Japan) and a motorized stage for centronucleated fibers evaluation. Centronucleated fibers were quantified using the Histolab software (Microvision, Evry, France).

Statistics. Data are presented as means ± SEM. Individual means between two groups were compared using the Mann–Whitney nonparametric test. Differences were considered to be statistically significant at $^*P < 0.05$.

SUPPLEMENTARY MATERIAL

Figure S1. Exon Splicing Enhancer (ESE) and Intron Splicing Enhancer (ISE) modifications.
Figure S2. Human and mouse dysferlin intron 48 homology.
Table S1. Primers used for PCRs on DNA and cDNA.
Table S2. Sequence of the different BD PTM Mex6 titin.
Table S3. Oligonucleotides used for mutagenesis.
Materials and Methods

ACKNOWLEDGMENTS

We would like to thank Eric Allemand, Philippe Moullier, François-Jérôme Authier, Fedor Svinartchouk, and Francis Quetier for helpful discussion. We are also grateful to Pierre Klein, Delphine Pion, and Yasmine Rabahi for excellent technical assistance.

REFERENCES

1. Mendell, JR, Rodino-Klapac, L, Sahenk, Z, Malik, V, Kaspar, BK, Walker, CM *et al.* (2012). Gene therapy for muscular dystrophy: lessons learned and path forward. *Neurosci Lett* **527**: 90–99.
2. Tang, Y, Cummins, J, Huard, J and Wang, B (2010). AAV-directed muscular dystrophy gene therapy. *Expert Opin Biol Ther* **10**: 395–408.
3. Hackman, P, Vihola, A, Haravuori, H, Marchand, S, Sarparanta, J, De Seze, J *et al.* (2002). Tibial muscular dystrophy is a titinopathy caused by mutations in TTN, the gene encoding the giant skeletal-muscle protein titin. *Am J Hum Genet* **71**: 492–500.
4. Udd, B, Vihola, A, Sarparanta, J, Richard, I and Hackman, P (2005). Titinopathies and extension of the M-line mutation phenotype beyond distal myopathy and LGMD2J. *Neurology* **64**: 636–642.
5. Udd, B, Kääriänen, H and Somer, H (1991). Muscular dystrophy with separate clinical phenotypes in a large family. *Muscle Nerve* **14**: 1050–1058.
6. Udd, B, Partanen, J, Halonen, P, Falck, B, Hakamies, L, Heikkilä, H *et al.* (1993). Tibial muscular dystrophy. Late adult-onset distal myopathy in 66 Finnish patients. *Arch Neurol* **50**: 604–608.
7. Liu, J, Aoki, M, Illa, I, Wu, C, Fardeau, M, Angelini, C *et al.* (1998). Dysferlin, a novel skeletal muscle gene, is mutated in Miyoshi myopathy and limb girdle muscular dystrophy. *Nat Genet* **20**: 31–36.
8. Bashir, R, Britton, S, Strachan, T, Keers, S, Vafiadaki, E, Lako, M *et al.* (1998). A gene related to Caenorhabditis elegans spermatogenesis factor fer-1 is mutated in limb-girdle muscular dystrophy type 2B. *Nat Genet* **20**: 37–42.
9. Le Roy, F, Charton, K, Lorson, CL and Richard, I (2009). RNA-targeting approaches for neuromuscular diseases. *Trends Mol Med* **15**: 580–591.
10. Havens, MA, Duelli, DM and Hastings, ML (2013). Targeting RNA splicing for disease therapy. *Wiley Interdiscip Rev RNA* **4**: 247–266.
11. Lorain, S, Peccate, C, Le Hir, M and Garcia, L (2010). Exon exchange approach to repair Duchenne dystrophin transcripts. *PLoS One* **5**: e10894.
12. Lorain, S, Peccate, C, Le Hir, M, Griffith, G, Philippi, S, Précigout, G *et al.* (2013). Dystrophin rescue by trans-splicing: a strategy for DMD genotypes not eligible for exon skipping approaches. *Nucleic Acids Res* **41**: 8391–8402.
13. Gruber, C, Koller, U, Murauer, EM, Hainzl, S, Hüttner, C, Kocher, T *et al.* (2013). The design and optimization of RNA trans-splicing molecules for skin cancer therapy. *Mol Oncol* **7**: 1056–1068.
14. Chao, H, Mansfield, SG, Bartel, RC, Hiriyanna, S, Mitchell, LG, Garcia-Blanco, MA *et al.* (2003). Phenotype correction of hemophilia A mice by spliceosome-mediated RNA trans-splicing. *Nat Med* **9**: 1015–1019.
15. Tahara, M, Pergolizzi, RG, Kobayashi, H, Krause, A, Luettich, K, Lesser, ML *et al.* (2004). Trans-splicing repair of CD40 ligand deficiency results in naturally regulated correction of a mouse model of hyper-IgM X-linked immunodeficiency. *Nat Med* **10**: 835–841.
16. Coady, TH and Lorson, CL (2010). Trans-splicing-mediated improvement in a severe mouse model of spinal muscular atrophy. *J Neurosci* **30**: 126–130.
17. Shababi, M, Glascock, J and Lorson, CL (2011). Combination of SMN trans-splicing and a neurotrophic factor increases the life span and body mass in a severe model of spinal muscular atrophy. *Hum Gene Ther* **22**: 135–144.
18. Avale, ME, Rodríguez-Martín, T and Gallo, JM (2013). Trans-splicing correction of tau isoform imbalance in a mouse model of tau mis-splicing. *Hum Mol Genet* **22**: 2603–2611.
19. Charton, K, Danièle, N, Vihola, A, Roudaut, C, Gicquel, E, Monjaret, F *et al.* (2010). Removal of the calpain 3 protease reverses the myopathology in a mouse model for titinopathies. *Hum Mol Genet* **19**: 4608–4624.
20. Corpet, F (1988). Multiple sequence alignment with hierarchical clustering. *Nucleic Acids Res* **16**: 10881–10890.
21. Castle, JC, Zhang, C, Shah, JK, Kulkarni, AV, Kalsotra, A, Cooper, TA *et al.* (2008). Expression of 24,426 human alternative splicing events and predicted cis regulation in 48 tissues and cell lines. *Nat Genet* **40**: 1416–1425.
22. Wang, J, Mansfield, SG, Cote, CA, Jiang, PD, Weng, K, Amar, MJ *et al.* (2009). Trans-splicing into highly abundant albumin transcripts for production of therapeutic proteins in vivo. *Mol Ther* **17**: 343–351.
23. Lostal, W, Bartoli, M, Roudaut, C, Bourg, N, Krahn, M, Pryadkina, M *et al.* (2012). Lack of correlation between outcomes of membrane repair assay and correction of dystrophic changes in experimental therapeutic strategy in dysferlinopathy. *PLoS One* **7**: e38036.
24. Puttaraju, M, DiPasquale, J, Baker, CC, Mitchell, LG and Garcia-Blanco, MA (2001). Messenger RNA repair and restoration of protein function by spliceosome-mediated RNA trans-splicing. *Mol Ther* **4**: 105–114.
25. Walls, ZF, Puttaraju, M, Temple, GF and Gambhir, SS (2008). A generalizable strategy for imaging pre-mRNA levels in living subjects using spliceosome-mediated RNA trans-splicing. *J Nucl Med* **49**: 1146–1154.
26. Kolmerer, B, Olivieri, N, Witt, CC, Herrmann, BG and Labeit, S (1996). Genomic organization of M line titin and its tissue-specific expression in two distinct isoforms. *J Mol Biol* **256**: 556–563.
27. Li, X, Eastman, EM, Schwartz, RJ and Draghia-Akli, R (1999). Synthetic muscle promoters: activities exceeding naturally occurring regulatory sequences. *Nat Biotechnol* **17**: 241–245.
28. Rodriguez-Martin, T, Garcia-Blanco, MA, Mansfield, SG, Grover, AC, Hutton, M, Yu, Q *et al.* (2005). Reprogramming of tau alternative splicing by spliceosome-mediated RNA trans-splicing: implications for tauopathies. *Proc Natl Acad Sci USA* **102**: 15659–15664.
29. Trapnell, C, Roberts, A, Goff, L, Pertea, G, Kim, D, Kelley, DR *et al.* (2012). Differential gene and transcript expression analysis of RNA-seq experiments with TopHat and Cufflinks. *Nat Protoc* **7**: 562–578.
30. Trapnell, C, Pachter, L and Salzberg, SL (2009). TopHat: discovering splice junctions with RNA-Seq. *Bioinformatics* **25**: 1105–1111.
31. Trapnell, C, Williams, BA, Pertea, G, Mortazavi, A, Kwan, G, van Baren, MJ *et al.* (2010). Transcript assembly and quantification by RNA-Seq reveals unannotated transcripts and isoform switching during cell differentiation. *Nat Biotechnol* **28**: 511–515.
32. Kim, D and Salzberg, SL (2011). TopHat-Fusion: an algorithm for discovery of novel fusion transcripts. *Genome Biol* **12**: R72.